

# Compressively Strained $\text{In}_x\text{Al}_{1-x}\text{N}/\text{Al}_{0.22}\text{Ga}_{0.78}\text{N}/\text{GaN}$ ( $x = 0.245-0.325$ ) Heterostructure Field Effect Transistors with Regrown AlGaN Contact Layers

Masanobu Hiroki\*, Narihiko Maeda, and Naoteru Shigekawa

NTT Photonics Laboratories, NTT Corporation, 3-1, Morinosato Wakamiya, Atsugi 243-0198, Japan

Received October 6, 2009; accepted November 19, 2009; published online April 20, 2010

Compressively strained  $\text{In}_x\text{Al}_{1-x}\text{N}$  (15 nm)/ $\text{Al}_{0.22}\text{Ga}_{0.78}\text{N}$  (3 nm)/GaN heterostructure field effect transistors (FETs) with regrown AlGaN contact layers were fabricated. The increase in compressive strain in InAlN reduced the polarization charge, i.e., the density of two-dimensional electron gas decreased from  $6.5 \times 10^{12}$  to  $1.3 \times 10^{12} \text{ cm}^{-2}$  as the In content of InAlN increased from 0.245 to 0.325. With the insertion of the AlGaN layer, electron mobility of as high as  $1570 \text{ cm}^2 \text{ V}^{-1} \text{ s}^{-1}$  was achieved at the In content of 0.245. Selectively regrown AlGaN contact layers reduced the sheet resistance from 17,000 to  $584 \Omega/\text{sq}$ . at the access layer for  $\text{In}_{0.325}\text{Al}_{0.675}\text{N}/\text{Al}_{0.22}\text{Ga}_{0.78}\text{N}/\text{GaN}$ . We fabricated FETs with this structure. The FETs without the regrown AlGaN contact layer did not operate at all owing to the high resistance. In contrast, the devices with the regrown AlGaN did. The maximum transconductance is 60 mS/mm, and the drain current is 0.11 A/mm. The threshold voltage becomes shallower, changing from  $-3.2$  to  $-0.2 \text{ V}$  with the increase in In content from 0.245 to 0.325. These results indicate that it is possible to fabricate enhancement-mode FETs with InAlN/AlGaN/GaN heterostructures. © 2010 The Japan Society of Applied Physics

DOI: 10.1143/JJAP.49.04DF13

## 1. Introduction

GaN-based field effect transistors (FETs) are attractive for high-frequency and high-power devices because of their high electron saturation velocity and high critical electric field. AlGaN/GaN heterostructures are conventionally used for FETs. A new material, InAlN, has the potential to replace the AlGaN barrier layer.<sup>1)</sup> The polarization effect is an important characteristic for III-nitride semiconductor heterostructures. A spontaneous and piezoelectric polarization induces an internal electric field because of the polarity of the wurtzite structure and the large electronegativity of nitrogen atoms.<sup>2,3)</sup> The large charge induced by the difference in the polarization between the barrier layer and the buffer layer gives rise to a high density of the two-dimensional electron gas (2DEG). Therefore, the density of 2DEG ( $N_S$ ), which affects the threshold voltage and sheet resistance, is varied by adjusting the composition and thickness of the barrier layer. When we use an InAlN barrier,  $N_S$  can be controlled over a wide range.

InAlN with In content of 0.17–0.18, lattice-matched to GaN, has a large spontaneous polarization charge of  $0.072 \text{ C/m}^2$ . This results in the generation of a large  $N_S$  of about  $2.5 \times 10^{13} \text{ cm}^{-2}$  at the heterointerface without lattice strain.<sup>1,4)</sup> Therefore, InAlN is attractive for fabricating FETs with low channel resistance and high reliability. As a result, there are many reports on lattice-matched (LM) InAlN.<sup>5–10)</sup>

On the other hand, compressively strained (CS) InAlN with In content higher than 0.18 is also interesting. For CS-InAlN/GaN heterostructures, the piezoelectric polarization is antiparallel to the spontaneous polarization. Therefore,  $N_S$  decreases with increasing In content. It has been predicted that the sum of the spontaneous and piezoelectric polarization charges should be equal to that of GaN for CS-InAlN with In content of about 0.32.<sup>4)</sup> In this case,  $N_S$  is eliminated at the heterointerface. Therefore, it is possible to fabricate enhancement-mode (E-mode) devices with CS-InAlN/GaN heterostructures. The reproducibility of the threshold voltage ( $V_{th}$ ) should be a large advantage in the fabrication of E-mode FETs with CS-InAlN/GaN heterostructures over conventional recessed-gate AlGaN/GaN structures.<sup>11)</sup> For

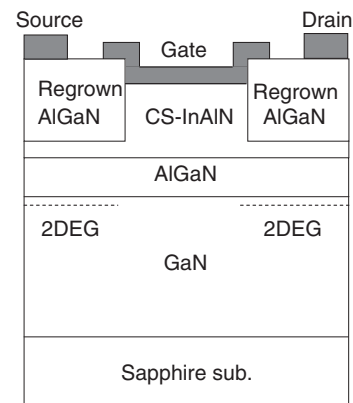


Fig. 1. Cross-sectional schematic view of InAlN/AlGaN/GaN FET with regrown AlGaN contact layer.

the recessed-gate structures,  $V_{th}$  is determined by the thickness of the AlGaN barrier layer. We must form a subnanometer-thick AlGaN barrier by a dry-etching process in order to achieve E-mode operation.  $V_{th}$  is largely varied with little variation of thickness; therefore, the accurate control of  $V_{th}$  is difficult for dry etching. In contrast, we can use the composition of InAlN to adjust  $V_{th}$  in a FET with the CS-InAlN barrier layer. This should provide better reproducibility because dry etching is not required. However, there are few reports on CS-InAlN/GaN heterostructures. In this study, we fabricated FETs with a CS-InAlN barrier layer and characterized the device performance.

One problem, however, with using CS-InAlN/GaN heterostructures to fabricate FETs is that the access resistance is extremely high. This is because the electron mobility is very low owing to alloy-disorder scattering.<sup>12)</sup> Also, there is either no or very little  $N_S$ . To solve these problems, we made two improvements to the device structure. Figure 1 shows a cross-sectional schematic view of the device structure in this study. First, we inserted a 3-nm-thick  $\text{Al}_{0.22}\text{Ga}_{0.78}\text{N}$  layer between InAlN and GaN to boost mobility. Generally, an AlN interlayer has been widely used<sup>5,6,8)</sup> to achieve high mobility. The AlN interlayer of a binary alloy can suppress alloy disorder scattering, and it increases the effective conduction-band offset because of

\*E-mail address: hiroki@aecl.ntt.co.jp

the large polarization charge.<sup>13,14</sup> The electron mobility is as high as  $1300 \text{ cm}^2 \text{ V}^{-1} \text{ s}^{-1}$  for InAlN/AlN/GaN heterostructures.<sup>8</sup> However, the surface tends to be rough. In addition, the insertion of an AlN interlayer has been shown to decrease the reliability of the AlGaN/GaN heterostructure FETs.<sup>15</sup> Recently, we obtained a flat surface and high electron mobility for InAlN/GaN heterostructures with an AlGaN interlayer.<sup>16,17</sup> In this study, we also used the AlGaN interlayer. In addition, we selectively regrew an AlGaN contact layer at the access region. With this technique, 2DEG is generated as a result of the polarization charge of the regrown AlGaN.

## 2. Experimental Procedure

The heterostructures were fabricated by low-pressure vertical metal organic vapor phase epitaxy (MOVPE) on sapphire substrates. Trimethylgallium, trimethylaluminum, trimethylindium, and ammonia were the precursors of Ga, Al, In, and N, respectively. First, we grew a 2- $\mu\text{m}$ -thick GaN buffer layer at about 1000 °C and 300 Torr. Next, we reduced the pressure to 200 Torr and deposited a 3-nm-thick layer of  $\text{Al}_{0.22}\text{Ga}_{0.78}\text{N}$ . Then, we cooled the wafers to 750–800 °C and switched the carrier gas from  $\text{H}_2$  to  $\text{N}_2$  for the growth of the InAlN layer, which has an In content of 0.245–0.325 and a thickness of 15 nm.

We fabricated FETs as follows. First, we deposited a 10-nm-thick  $\text{SiO}_2$  mask on the samples and formed a 2- $\mu\text{m}$ -long  $\text{SiO}_2$  stripe on the gate region by  $\text{SF}_6$  reactive ion etching. Next, we removed the InAlN in the access region down to a thickness of 10 nm by  $\text{Cl}_2$  inductively coupled plasma etching. Then, we selectively regrew 26-nm-thick  $\text{Al}_{0.26}\text{Ga}_{0.74}\text{N}$  on the access region by MOVPE. The growth temperature and pressure were 1000 °C and 300 Torr, respectively. Finally, we formed a mesa structure and the electrode. The gate electrode was Ni/Au and the ohmic electrode was Ti/Al/Ti/Au annealed at 850 °C for 30 s. The gate length and width were 4 and 20  $\mu\text{m}$ , respectively. The source–drain space was 8  $\mu\text{m}$ .

We observed the surface morphology by atomic force microscopy (AFM) and estimated  $N_S$  and the electron mobility from nondestructive eddy current measurements. We characterized the composition of InAlN by X-ray diffraction (XRD) analysis. The sheet resistance was estimated by the transmission line method (TLM). The DC characteristics of the FETs were measured with a semiconductor parameter analyzer.

## 3. Results and Discussion

### 3.1 Properties of InAlN/AlGaN/GaN heterostructures

First, we evaluated the crystal quality of CS-InAlN. Figure 2 shows the XRD curves of the InAlN/AlGaN/GaN heterostructures with In contents from 0.245 to 0.325. Clear InAlN peaks and fringes appear for all samples, which means that the samples have an abrupt heterointerface. No phase separation is observed in these curves. Figure 3 shows AFM images of the surface morphology of CS- $\text{In}_x\text{Al}_{1-x}\text{N}/\text{Al}_{0.22}\text{Ga}_{0.78}\text{N}/\text{GaN}$  ( $x = 0.245, 0.29, 0.307, \text{ and } 0.325$ ). When the In content is 0.245, the surface is smooth. The rms roughness is as low as about 0.3 nm. The obtained morphology, which has monolayer steps and atomically fluctuated terraces, is nearly the same as that of LM-

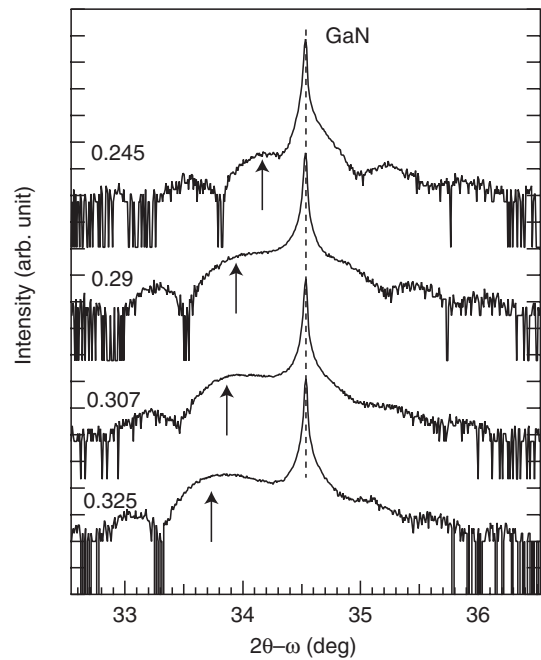


Fig. 2. XRD curves of  $\text{In}_x\text{Al}_{1-x}\text{N}$  (15 nm)/ $\text{Al}_{0.22}\text{Ga}_{0.78}\text{N}$  (3 nm)/GaN ( $x = 0.245, 0.29, 0.307, \text{ and } 0.325$ ). Arrows indicate InAlN peaks.

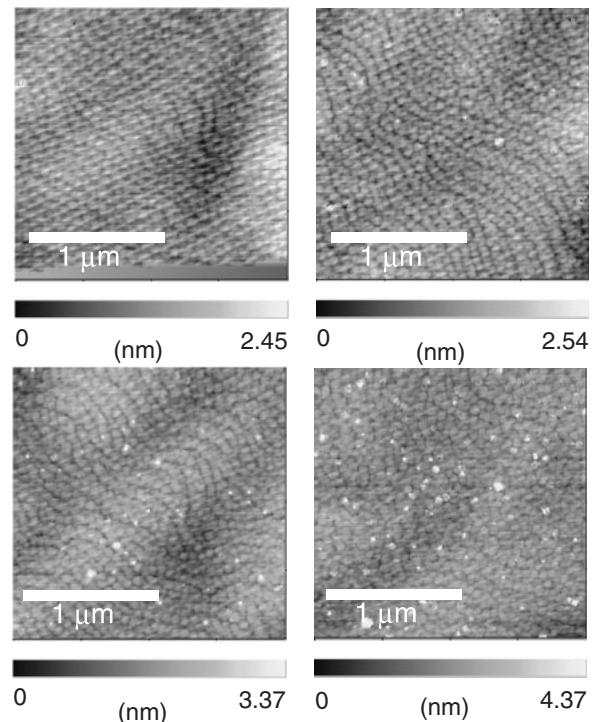
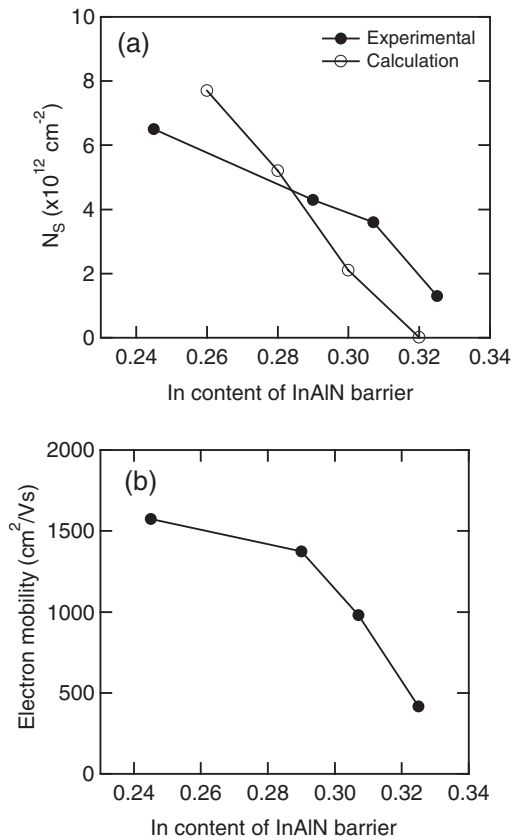


Fig. 3. AFM images of surface morphology of compressively strained InAlN/AlGaN/GaN heterostructures with In contents of 0.245, 0.29, 0.307, and 0.325.

InAlN.<sup>16</sup> However, bumplike defects appear when the In content is 0.29 or higher. Also, the density increases as the In content increases. Although the precise reason for this is not clear, the appearance of defects is associated with the large compressive strain. We must improve the crystal growth conditions to eliminate the defects.

Next, we estimated the electrical properties of the heterostructures from the non-destructive eddy current measurements. Figure 4 shows  $N_S$  and electron mobility



**Fig. 4.** (a)  $N_S$  and (b) electron mobility of  $\text{In}_x\text{Al}_{1-x}\text{N}$  (15 nm)/ $\text{Al}_{0.22}\text{Ga}_{0.78}\text{N}$  (3 nm)/GaN heterostructures as a function of In content. In (a), closed and open circles show experimental and calculated results, respectively.

as a function of the In content of the InAlN barrier layer.  $N_S$  decreased from  $6.5 \times 10^{12}$  to  $1.3 \times 10^{12} \text{ cm}^{-2}$  as the In content increased from 0.245 to 0.325, resulting from the decrease in the sum of the piezoelectric and spontaneous polarization charges. Figure 4(a) also shows the calculated results obtained by self-consistently solving the one-dimensional Schrödinger and Poisson equations.<sup>18)</sup> These values are different from the experimental ones. For the calculation, we used physical parameters such as the band gap, band offset, Schottky barrier height, polarization charge, and bowing parameters from refs. 4 and 19. Some predicted parameter values probably differ from the actual ones.  $N_S$  should be eliminated for InAlN/GaN heterostructures when the In content is 0.325; however, 2DEG is still generated as a result of the insertion of AlGaIn. To achieve E-mode operation for FET, we must redesign the barrier structure, particularly the thickness of the AlGaIn layer, because it strongly affects the threshold voltage, as discussed later. However, the AlGaIn layer is indispensable for boosting electron mobility, which is greatly reduced by the large alloy-disorder scattering rate of InAlN for InAlN/GaN.<sup>12)</sup> The insertion of AlGaIn is effective for suppression of alloy-disorder scattering and for obtaining an abrupt heterointerface. We achieved a high mobility of  $1,570 \text{ cm}^2 \text{ V}^{-1} \text{ s}^{-1}$  when the In content was 0.245. However, it decreased to  $416 \text{ cm}^2 \text{ V}^{-1} \text{ s}^{-1}$  as the In content increased to 0.325. The surface becomes rougher for higher In content (Fig. 3); however, we consider that the reduction is not due to the deterioration of the heterointerface for the following reasons.

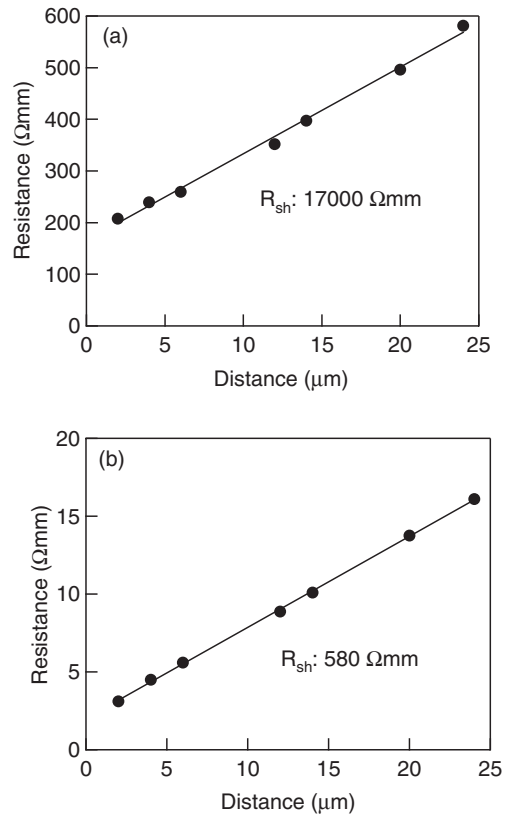


**Fig. 5.** TLM results for  $\text{In}_{0.325}\text{Al}_{0.675}\text{N}$  (15 nm)/ $\text{Al}_{0.22}\text{Ga}_{0.78}\text{N}$  (3 nm)/GaN heterostructures (a) with regrown AlGaIn and (b) without regrown AlGaIn contact layers.

(1) The abruptness of the heterointerface is not different among these samples because of the insertion of the AlGaIn layer. (2) The influence of interface roughness on the mobility of 2DEG becomes lower as  $N_S$  decreases.<sup>20)</sup> Generally, the contribution of Coulomb scattering probably becomes dominant for low  $N_S$  because the screening effect becomes weak. The mobility decreases when  $N_S$  becomes lower than  $7 \times 10^{12} \text{ cm}^{-2}$  for AlGaIn/GaN heterostructures.<sup>21,22)</sup> Therefore, we consider that the low electron mobility for InAlN/AlGaIn/GaN with high In content is due to Coulomb scattering. In addition, the density of residual donors might increase in the InAlN layer with higher In content owing to the large compressive strain. The increase in residual donor density might also result in the decrease of mobility. However, the low mobility of  $\text{In}_{0.325}\text{Al}_{0.675}\text{N}/\text{Al}_{0.22}\text{Ga}_{0.78}\text{N}/\text{GaN}$  should not degrade the performance of the FETs in this study (Fig. 1). At the gate region, Coulomb scattering should not be dominant in the high electric field in on-state FETs. In the access region, the mobility should be higher again because  $N_S$  is generated by the selectively regrown AlGaIn, as mentioned later.

### 3.2 Device characteristics of the InAlN/AlGaIn/GaN heterostructure FETs

We estimated the resistance in the access region with the selectively regrown AlGaIn contact layer. Figure 5 shows the TLM measurement data for  $\text{In}_{0.325}\text{Al}_{0.675}\text{N}/\text{Al}_{0.22}\text{Ga}_{0.78}\text{N}/\text{GaN}$  with and without regrown AlGaIn. We found that the resistance drastically decreases as a result of the AlGaIn regrowth. The sheet resistance ( $R_{sh}$ ) estimated

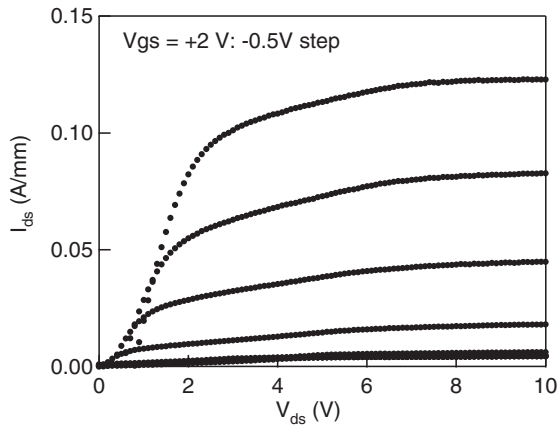


Fig. 6.  $I$ - $V$  characteristics of  $\text{In}_{0.325}\text{Al}_{0.675}\text{N}$  (15 nm)/ $\text{Al}_{0.22}\text{Ga}_{0.78}\text{N}$  (3 nm)/GaN heterostructure FETs.

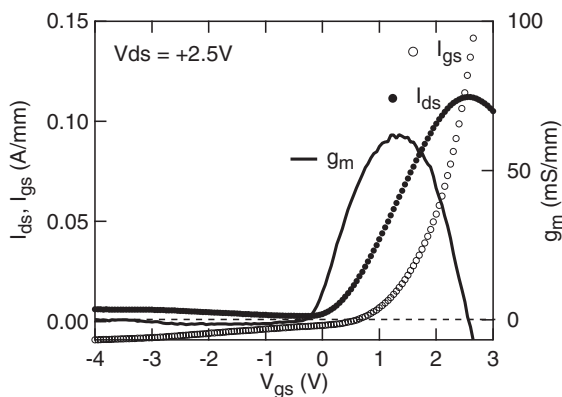


Fig. 7. Transfer characteristics of  $\text{In}_{0.325}\text{Al}_{0.675}\text{N}$  (15 nm)/ $\text{Al}_{0.22}\text{Ga}_{0.78}\text{N}$  (3 nm)/GaN heterostructure FETs. Closed circles, open circles, and a solid line show drain-source current, gate-source current, and transconductance, respectively.

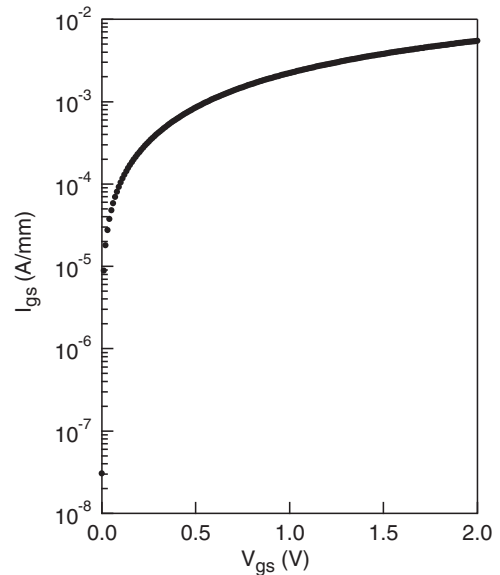


Fig. 8. Forward gate leakage characteristics of  $\text{In}_{0.325}\text{Al}_{0.675}\text{N}$  (15 nm)/ $\text{Al}_{0.22}\text{Ga}_{0.78}\text{N}$  (3 nm)/GaN heterostructure FETs.

from the slope obtained by the TLM is  $17,000 \Omega/\text{sq.}$  for the sample without regrown AlGaIn. In contrast,  $R_{\text{sh}}$  is  $587 \Omega/\text{sq.}$  with the regrown layer. The generation of 2DEG and an increase in mobility are found.  $R_{\text{sh}}$  can be reduced when we optimize the thickness and composition of regrown AlGaIn or the etching depth of InAlIn. The contact resistance is  $1.0 \Omega/\text{mm}$ . It can also be reduced by Si doping, as previously reported.<sup>23-25)</sup>

Next, we observed the DC characteristics of the FETs. Figures 6-8 show the  $I$ - $V$ , transfer, and forward gate leakage characteristics of  $\text{In}_{0.325}\text{Al}_{0.675}\text{N}/\text{Al}_{0.22}\text{Ga}_{0.78}\text{N}/\text{GaN}$  heterostructure FETs, respectively. The FETs without the regrown AlGaIn contact layer did not operate at all owing to the high resistance of the channel. In contrast, the devices with regrown AlGaIn operated, as seen in Fig. 6. However, the performance is still low. A large leakage current of about  $5 \text{ mA}/\text{mm}$  is observed in the pinch-off state. The maximum transconductance ( $g_m$ ) is as low as  $60 \text{ mS}/\text{mm}$ , and the maximum drain-source current ( $I_{\text{ds}}$ ) is only  $0.11 \text{ A}/\text{mm}$ . This is due to the large gate leakage current. The gate-source current ( $I_{\text{gs}}$ ) (Fig. 7) is appreciably large.  $I_{\text{gs}}$  is as large as  $-10 \text{ mA}/\text{mm}$  at a gate-source voltage ( $V_{\text{gs}}$ ) of  $-4 \text{ V}$ . The leakage current through the gate source and through through gate drain is attributed to the large  $I_{\text{ds}}$  in the pinch-off state. The forward gate leakage of the FETs is

considerably larger than that for the AlGaIn/GaN of LM-InAlIn/GaN. The forward gate current is not Schottky-like and is leaky in the bias region (Fig. 8).  $I_{\text{gs}}$  rapidly increased when  $V_{\text{gs}}$  exceeded  $0.5 \text{ V}$ , and it exceeded  $I_{\text{ds}}$  at a  $V_{\text{gs}}$  of  $2.5 \text{ V}$ . This results in low  $I_{\text{ds}}$  and low  $g_m$ . Although it is not clear why the gate leakage is so large, we consider two reasons at the present stage. One is surface damage caused during AlGaIn regrowth. The high regrowth temperature should oxidize the InAlIn surface on the gate region with the  $\text{SiO}_2$  mask. The oxidation would probably generate a high density of surface defects.<sup>26,27)</sup> In this case, replacing  $\text{SiO}_2$  with a nonoxide material, such as  $\text{Si}_3\text{N}_4$ , may be promising. The other is the leakage through the interface between the InAlIn barrier and regrown AlGaIn contact layer. Anyway, we must reduce gate leakage in order to achieve high device performance. Inserting an insulator between the gate and InAlIn, to form what is called a metal insulator semiconductor (MIS) structure, is one possible way of obtaining high performance.

Finally, we discuss  $V_{\text{th}}$ . Figure 9 shows  $V_{\text{th}}$  as a function of the In content of the InAlIn barrier layer.  $V_{\text{th}}$  is defined by extrapolating  $g_m$ . As previously mentioned,  $N_{\text{S}}$  decreased from  $6.5 \times 10^{12}$  to  $1.3 \times 10^{12} \text{ cm}^{-2}$  as the In content of InAlIn increased from 0.245 to 0.325 (Fig. 4). In this range,  $V_{\text{th}}$  becomes shallower, changing from  $-3.2$  to  $-0.2 \text{ V}$ . We did not achieve E-mode operation in this study, even when the In content was 0.325. We must redesign the barrier structure. Therefore, we investigated how  $V_{\text{th}}$  depends on the barrier layer thickness. Figure 10 shows the calculated  $N_{\text{S}}$  variation caused by gate voltage in the  $\text{In}_{0.32}\text{Al}_{0.68}\text{N}/\text{Al}_{0.22}\text{Ga}_{0.78}\text{N}/\text{GaN}$  heterostructures.  $V_{\text{th}}$  is not varied by thinning the InAlIn barrier, as seen in Fig. 10(a). Since the low polarization charge of  $\text{In}_{0.32}\text{Al}_{0.68}\text{N}$  makes the potential profile in this barrier flat (Fig. 11), the potential height at the channel is not affected by the thickness of InAlIn. In contrast, thinning  $\text{Al}_{0.22}\text{Ga}_{0.78}\text{N}$ , which has a larger polarization charge than  $\text{In}_{0.32}\text{Al}_{0.68}\text{N}$ , is effective for making  $V_{\text{th}}$  shallower [Fig. 10(b)]. A  $V_{\text{th}}$  increase of  $0.2 \text{ V}$  can be expected by  $1 \text{ nm}$  thinning of  $\text{Al}_{0.22}\text{Ga}_{0.78}\text{N}$ . However, we

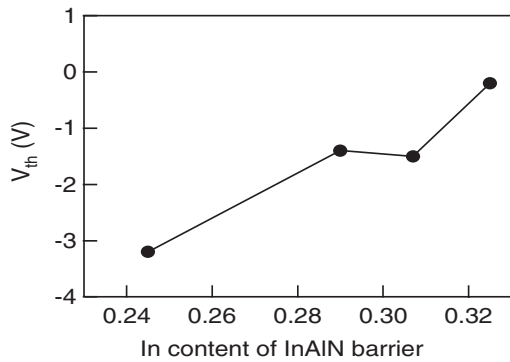


Fig. 9. Threshold voltage for  $In_xAl_{1-x}N$  (15 nm)/ $Al_{0.22}Ga_{0.78}N$  (3 nm)/GaN heterostructure FETs as a function of In content.

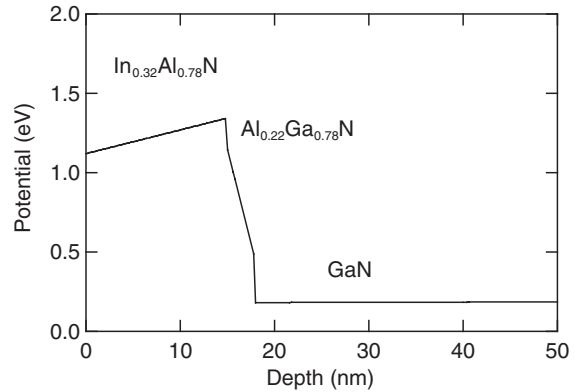


Fig. 11. Depth profile of conduction band potential in  $In_{0.32}Al_{0.68}N/Al_{0.22}Ga_{0.78}N/GaN$  heterostructures.

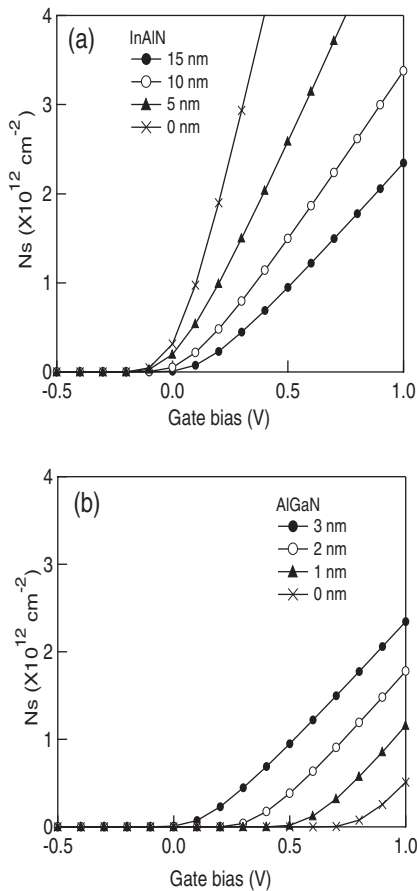


Fig. 10. Gate bias dependence of  $N_s$  for  $In_{0.32}Al_{0.68}N/Al_{0.22}Ga_{0.78}N/GaN$  heterostructures obtained by calculation when (a) the thickness of InAlN is varied from 0 to 15 nm and (b) that of AlGaN is varied from 0 to 3 nm.

must pay attention to the reduction of the electron mobility that such thinning would cause. The suppression effect of alloy-disorder scattering will be weaker when we thin AlGaN. We must optimize the trade-off between electron mobility and  $V_{th}$ .

4. Conclusions

CS- $In_xAl_{1-x}N$  (15 nm)/ $Al_{0.22}Ga_{0.78}N$  (3 nm)/GaN heterostructure FETs with regrown AlGaN contact layers were fabricated. We found that the compressive strain in InAlN reduced the polarization charge in the heterostructures.  $N_s$  decreased from  $6.5 \times 10^{12}$  to  $1.3 \times 10^{12} \text{ cm}^{-2}$  as the

In content of InAlN increased from 0.245 to 0.325. With the insertion of the AlGaN layer, electron mobility of as high as  $1570 \text{ cm}^2 \text{ V}^{-1} \text{ s}^{-1}$  was achieved at the In content of 0.245. Selectively regrown AlGaN contact layers reduced the sheet resistance from 17,000 to  $584 \Omega/\text{sq.}$  at the access layer for  $In_{0.325}Al_{0.675}N/Al_{0.22}Ga_{0.78}N/GaN$ . The FETs without the regrown AlGaN contact layer did not operate at all because of the high resistance. In contrast, the devices with the regrown AlGaN did. However, the device performance was still low owing to the large gate leakage current. The maximum  $g_m$  is 60 mS/mm, and  $I_{ds}$  is 0.11 A/mm. The threshold voltage becomes shallower, changing from  $-3.2$  to  $-0.2 \text{ V}$  with the increase in In content from 0.245 to 0.325. Calculation results indicate that reducing the thickness of the AlGaN interlayer is effective for making  $V_{th}$  shallower. These results indicate that the CS-InAlN barrier may make it possible to obtain E-mode GaN-based FETs.

Acknowledgments

The authors thank Drs. Kazuhide Kumakura, Makoto Kasu, and Toshiki Makimoto for their assistance in MOVPE growth, and Drs. Shoji Yamahata, Takatomo Enoki, and Yoshinori Hibino for their support and encouragement throughout this work.

- 1) J. Kuzmík: *IEEE Electron Device Lett.* **22** (2001) 510.
- 2) A. Bykhovski, B. Gelmont, and M. Shur: *J. Appl. Phys.* **74** (1993) 6734.
- 3) F. Bernardini and V. Fiorentini: *Phys. Rev. B* **56** (1997) 10024.
- 4) O. Ambacher, R. Dimitrov, M. Stutzmann, B. E. Foutz, M. J. Murphy, J. A. Smart, J. R. Shealy, N. G. Weimann, K. Chu, M. Chumbes, B. Green, A. J. Sierakowski, W. J. Schaff, and L. F. Eastman: *Phys. Status Solidi B* **216** (1999) 381.
- 5) M. Higashiwaki and T. Matsui: *Jpn. J. Appl. Phys.* **43** (2004) L768.
- 6) A. Dadgar, F. Schulze, J. Bläsing, A. Diez, A. Krost, M. Neuberger, E. Kohn, I. Daumiller, and M. Kunze: *Appl. Phys. Lett.* **85** (2004) 5400.
- 7) O. Katz, D. Mistele, B. Meyler, G. Bahir, and J. Salzman: *Electron. Lett.* **40** (2004) 1304.
- 8) M. Gonschorek, J.-F. Carlin, E. Feltn, M. A. Py, and N. Grandjean: *Appl. Phys. Lett.* **89** (2006) 062106.
- 9) K. Jegannathan, M. Shimizu, H. Okumura, Y. Yano, and N. Akutsu: *J. Cryst. Growth* **304** (2007) 342.
- 10) M. Miyoshi, Y. Kuraoka, M. Tanaka, and T. Egawa: *Appl. Phys. Express* **1** (2008) 081102.
- 11) V. Kumar, A. Kuliev, T. Tanaka, Y. Otoki, and I. Adesida: *Electron. Lett.* **39** (2003) 1758.

- 12) V. W. L. Chin, B. Zhou, T. L. Tansley, and X. Lin: *J. Appl. Phys.* **77** (1995) 6064.
- 13) I. P. Smorchkova, L. Chen, T. Mates, L. Shen, S. Heikman, B. Moran, S. Keller, S. P. DenBaars, J. S. Speck, and U. K. Mishra: *J. Appl. Phys.* **90** (2001) 5196.
- 14) L. Shen, S. Heikman, B. Moran, R. Coffie, N.-Q. Zhang, D. Buttari, I. P. Smorchkova, S. Keller, S. P. DenBaars, and U. K. Mishra: *IEEE Electron Device Lett.* **22** (2001) 457.
- 15) R. Coffie, Y. C. Chen, I. Smorchkova, M. Wojtowicz, Y. C. Chou, B. Heying, and A. Oki: 44th Ann. IEEE Int. Reliability Physics Symp. Proc., 2006, p. 99.
- 16) M. Hiroki, N. Maeda, and T. Kobayashi: *Appl. Phys. Express* **1** (2008) 111102.
- 17) M. Hiroki, N. Maeda, and T. Kobayashi: *Phys. Status Solidi C* **6** (2009) 1056.
- 18) 1D Poisson–Schrödinger solver program developed by Dr. Gregory Snider and University of Notre Dame [<http://www.nd.edu/~gsnider/>].
- 19) W. Walukiewicz, S. X. Li, J. Wu, K. M. Yu, J. W. Ager III, E. E. Haller, H. Lu, and J. S. William: *J. Cryst. Growth* **269** (2004) 119.
- 20) D. Zanato, S. Gokden, N. Balkan, B. K. Ridley, and W. J. Schaff: *Semicond. Sci. Technol.* **19** (2004) 427.
- 21) R. Gaska, M. S. Shur, A. D. Bykhovski, A. O. Orlov, and G. L. Snider: *Appl. Phys. Lett.* **74** (1999) 287.
- 22) J. Antoszewski, M. Gracey, J. M. Dell, L. Faraone, T. A. Fisher, G. Parish, Y.-F. Wu, and U. K. Mishra: *J. Appl. Phys.* **87** (2000) 3900.
- 23) S. Heikman, S. P. DenBaars, and U. K. Mishra: *Jpn. J. Appl. Phys.* **40** (2001) 565.
- 24) S. Heikman, S. Keller, S. P. DenBaars, and U. K. Mishra: *Appl. Phys. Lett.* **78** (2001) 2876.
- 25) N. Maeda, T. Saitoh, K. Tsubaki, and N. Kobayashi: *Phys. Status Solidi A* **188** (2001) 223.
- 26) X. Hu, A. Koudymov, G. Simin, J. Yang, M. A. Khan, A. Tarakji, M. S. Shur, and R. Gaska: *Appl. Phys. Lett.* **79** (2001) 2832.
- 27) T. Hashizume and H. Hasegawa: *Appl. Surf. Sci.* **234** (2004) 387.